Electrostatics at the oil–water interface, stability, and order in emulsions and colloids

Mirjam E. Leunissen*†, Alfons van Blaaderen*†, Andrew D. Hollingsworth‡§¶, Matthew T. Sullivan§‖**, and Paul M. Chaikin†§¶‖

*Soft Condensed Matter, Debye Institute, Utrecht University, Princetonplein 5, 3584 CC, Utrecht, The Netherlands; and ‡Department of Chemical Engineering, §Princeton Institute for the Science and Technology of Materials, and ‖Department of Physics, Princeton University, Princeton, NJ 08534

Contributed by Paul M. Chaikin, December 4, 2006 (sent for review August 12, 2006)

Oil–water mixtures are ubiquitous in nature and are particularly important in biology and industry. Usually additives are used to prevent the liquid droplets from coalescing. Here, we show that stabilization can also be obtained from electrostatics, because of the well known remarkable properties of water. Preferential ion uptake leads to a tunable droplet charge and surprisingly stable, additive-free, water-in-oil emulsions that can crystallize. For particle-stabilized ("Pickering") emulsions we find that even extremely hydrophobic, nonwetting particles can be strongly bound to (like-charged) oil–water interfaces because of image charge effects. These basic insights are important for emulsion production, encapsulation, and (self-)assembly, as we demonstrate by fabricating a diversity of structures in bulk, on surfaces, and in confined geometries.

colloidosomes | Pickering | Wigner crystal | self-assembly | low polar

The stabilization of emulsions and colloidal particle suspensions against aggregation and phase separation is an ancient problem. Whereas "emulsifiers," for example, surfactants and small particles, are commonly used to prepare stable oil–water mixtures, solid colloids often are stabilized by a charge on their surface (1–3). Charged entities are expected in high dielectric constant (ε) liquids, such as water ($\varepsilon \approx 80$), where the energetic penalty for charge separation is small. Recently, however, the focus has shifted to low dielectric constant media, in which electrostatics can also play a surprisingly dominant role (4–10), producing fascinating phenomena like the extraordinary crystal in Fig. 1*A*. Here, poly(methylmethacrylate) (PMMA) spheres (radius $a_c = 1.08$ μm) were suspended in a density matching mixture of cyclohexyl bromide (CHB) and *cis*-decalin (CHB-decalin; $\varepsilon \approx 5.6$). They form body-centered-cubic Coulomb or "Wigner" crystals, with lattice constants up to 40 μm (5), similar to one-component plasmas (11). Importantly, in this low-polar solvent, charge dissociation still occurs spontaneously (7), contrary to truly apolar media ($\varepsilon \sim 2$) that require charge stabilizing surfactants (6, 8). Although electrophoresis (see *Materials and Methods*) shows that the particles carry a significant charge, $Z \approx +450\,e$ (where e is the elementary charge), such extremely large lattice constants are surprising. Assuming a screened Coulomb pair potential (12)††, the particle interaction range will depend on the ion concentration, n, in the solvent through the Debye screening length, $\kappa^{-1} \propto n^{-1/2}$. Wigner crystals require an extremely low ionic strength, so that the screening length is many particle diameters and the interaction almost purely Coulombic. We estimate $\kappa^{-1} \approx 1.6$ μm only, for CHB-decalin (see *Materials and Methods*), but discovered that the presence of water (even minute quantities) reproducibly induces these crystals by tremendously increasing the screening length. Apparently, the immiscible water phase acts as an "ion sink" for the charged species in the oily solvent. These intriguing observations led to the following studies on the role of electrostatics in oil–water mixtures.

Results and Discussion

When brought into contact, water and the oily solvent CHB(-decalin) form an interface. Just considering the electrostatic self-energy $e^2/\varepsilon\varepsilon_0 a_i$ of a monovalent ion (radius a_i) in solution, ions from the oil should strongly partition into the higher dielectric constant water phase. The exact influence of the various ion–solvent interactions is more difficult to estimate, but strong specific interactions, such as hydrogen bonding, enhance the affinity for water even further (13, 14).

This ion-absorbing activity is clearly demonstrated by straightforward conductivity measurements: upon 24 h of contact with an equal volume of water the conductivity, σ, of 50 ml of CHB (as received) decreased from 6,760 to 700 pS/cm. Because of their small volume, we could not directly measure the conductivity of the water–oil combinations in our small microscopy cells. However, from a comparison with the "bulk" results listed above we estimate that in this case the latter number will be ≈40 times lower, as we started with a purified CHB-decalin mixture, which has a lower conductivity already ($\sigma = 165$ pS/cm). This estimate is supported by a rough measurement of the typical relaxation time, $\tau = \varepsilon\varepsilon_0/\sigma$, inside these small capillaries, which indeed points to very low conductivities, in the range of 1–10 pS/cm. We deem it likely that full equilibrium is reached in 24 h, as no further change in the colloid structure inside the oily phase (see below) was observed after this time. Note that this partitioning process is not specific to the water–CHB couple, but is a universal phenomenon, which is easily understood when equating the electrochemical potentials of the ions in the two phases (15). Nevertheless, its consequences are rarely considered in emulsion research, despite the recognition of its importance in, for example, phase-transfer catalysis (16).

The ion partitioning described above and other effects caused by the water–oil permittivity difference readily show up in oil–water mixtures to which we added colloidal particles. Fig. 1*B* shows a large interface between an oily colloidal suspension and

Author contributions: A.v.B. and P.M.C. designed research; M.E.L., A.D.H., and M.T.S. performed research; A.D.H. contributed new reagents/analytic tools; M.E.L., A.v.B., and P.M.C. analyzed data; and M.E.L. and P.M.C. wrote the paper.

The authors declare no conflict of interest.

Freely available online through the PNAS open access option.

Abbreviations: PMMA, poly(methylmethacrylate); CHB, cyclohexyl bromide; RITC, rhodamine isothiocyanate.

†To whom correspondence may be addressed. E-mail: m.e.leunissen@phys.uu.nl, a.vanblaaderen@phys.uu.nl, or chaikin@physics.nyu.edu.

¶Present address: Department of Physics, Center for Soft Matter Research, New York University, New York, NY 10003.

**Present address: Department of Engineering and Applied Sciences, Harvard University, Cambridge, MA 02138.

††In our earlier work on similar suspensions, though with less extreme screening lengths (10), the behavior was well described by the solution of the Poisson-Boltzmann equation for low, constant surface potentials: $V(r) = (Z^2e^2/4\pi\varepsilon\varepsilon_0)[e^{Ka_c}/(1 + Ka_c)]^2(e^{-Kr}/r)$, with r the interparticle distance, ε_0 the dielectric permittivity of vacuum, and $K^{-1} = (ne^2/\varepsilon\varepsilon_0 k_B T)^{-1/2}$ the Debye screening length, where n is the (monovalent) ion concentration, k_B is Boltzmann's constant, and T is the absolute temperature. For the present suspensions the real situation likely lies in between the constant surface charge and constant surface potential limits.

This article contains supporting information online at www.pnas.org/cgi/content/full/0610589104/DC1.

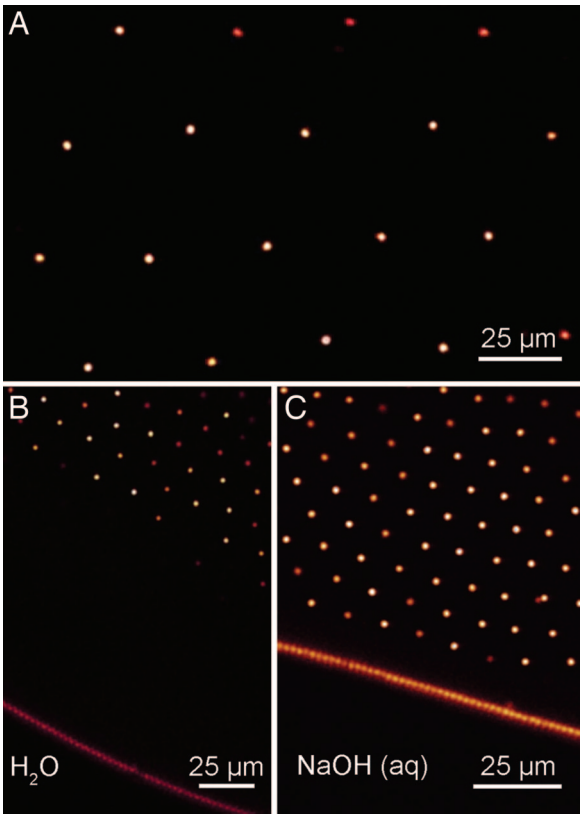

Fig. 1. Confocal micrographs of PMMA spheres (radius 1.08 μm) suspended in CHB-decalin, in contact with water. (*A*) Part of a (110) plane of the body-centered-cubic colloidal crystal in the bulk oil phase. (*B*) Particle monolayer, followed by a large zone depleted of particles near the water-suspension interface. (*C*) With 1.6 μM NaOH in the water phase the depleted zone in the oil phase shrinks considerably.

water. Aside from the Wigner crystal of colloidal particles in the oil phase there are two remarkable features: a particle monolayer near the interface and a large zone ($\approx$50–100 μm) depleted of particles. As the charge of the interfacial particles is effectively cancelled by its image in the water phase (see below), it must be a net charge of the water phase itself that repels the particles in the oil phase.

As mentioned before, water, as compared with oil, is a more favorable environment for any simple ion. However, certain species are preferred, as they all have different affinities (13, 14). Here, the major constituent ions are OH^-, H^+, and Br^-, with the latter originating from the (partial) dissociation of the HBr decomposition product of CHB (produced in a radical dehalogenation reaction). Although the dissociation equilibrium constants and solvation free energies in CHB are not known, we hypothesize that H^+ has the strongest affinity for water. Its hydration free energy [$-1{,}099$ kJ/mol, versus -437.5 and -326.6 kJ/mol for OH^- and Br^-, respectively (17, 18)] contains a large hydrogen-bonding contribution, which is unlikely to be counterbalanced by the ion–solvent interactions in the oily CHB phase. This scenario of preferential ion partitioning would produce positively charged water droplets, as is confirmed by their observed direction of electrophoretic motion (see *Materials and Methods*). Moreover, a moderate potential (of the order of 100 mV) could suffice already to explain the large distance over which the like-charged particles in the oily colloidal suspension of Fig. 1*B* are repelled by the water phase. To estimate this potential we used the expressions derived in ref. 19, for the interaction of a single small colloidal particle with an impermeable interface, as an approximation (additional work is needed for a better theoretical description of our experimental system, taking into account the double layers in both the oil and water phases and the fact that the colloidal particles are part of a macroscopic crystal).

With OH^- and H^+ present, it is not surprising that we can tune the droplet charge through the pH, shifting the dissociation and partitioning equilibria. Fig. 1*C* shows a NaOH-containing droplet (pH 8.2) in contact with the oily colloidal suspension. Note the near absence of the depleted zone, whereas the colloidal crystal remains the same, indicating that the ion drainage continues. In accordance with this observation, we now find that the water droplets are nearly neutral. Finally, we point out that the mechanism of preferential ion partitioning as described above is different from the interfacial OH^- adsorption through which (low ε) oil droplets sometimes are thought to acquire their (negative) charge (20, 21), as it does not involve specific interactions between the ions and the interface and depends on all ionic species present.

We now consider the layer of colloidal particles near the oil–water interface, a feature of particle-stabilized emulsions. It is often thought that partial wetting of the particles is essential for their interfacial binding in such "Pickering" emulsions (3, 22). Remarkably, our PMMA particles in CHB-decalin are almost nonwet by the water phase, as is apparent from Fig. 2 *A* and *B* (i.e., the particles sit at and not in the interface). Measurement of the three-phase contact angle at a macroscopic PMMA surface (see *Materials and Methods*) often yielded values of nearly 180°, although occasionally values as low as 165° are observed (Fig. 3 *A* and *B*). However, a particle in the oil phase brought within $\approx$2 μm of a like-charged water interface, was pulled from our optical tweezers to the interface. This finding indicates a strong long-range attractive force, possibly on top of a (small) wetting effect.

The explanation for these observations again lies in the large dielectric constant difference of the oil and water phases. When a charged particle approaches the interface of a conductor, an image charge of opposite sign appears at the mirror position and an attraction results (23). In case of a conducting (water) sphere of radius R in a dielectric (oil) medium (ε_m), a point particle of charge Z (colloid) at a distance d from the droplet center induces an image charge $Z' = -(R/d)Z$ at position $R' = (1/d)R^2$. Assuming that the water droplet charge, Q, has the same sign as the colloidal particle charge and ignoring screening and possible van der Waals interactions, the net interaction sums up to:

$$V(d) = \frac{Z}{\varepsilon_m \varepsilon_0}\left(\frac{Q}{d} - \frac{ZR}{(R^2 - d^2)}\right). \qquad [1]$$

From this simplified description it becomes clear that as the particle approaches the charged interface, $d \to R$ and the image charge attraction always dominates. Recently, Danov *et al.* (24) derived the image charge interaction for finite-sized particles (neglecting the double layer in the oil phase). They found that the (long-range) attraction became very strong for small, submicrometer particles, with interaction energies orders of magnitude larger than the thermal energy. Nevertheless, only a few experimental measurements of image charge interactions in oil–water mixtures can be found in the literature (e.g., in ref. 25, where it contributes to the interaction potential between interfacial particles), and we are not aware of any previous demonstrations of their importance in the actual binding of the particles to the interface. Our oil–water mixtures with nonwet particles, however, effectively separate the image charge effects from surface tension contributions.

Besides the PMMA/CHB/water combination, we found several other systems with strongly bound nonwet particles. For instance, Hyflon PFA particles (radius $a_c \approx 90$ nm) in CHB form

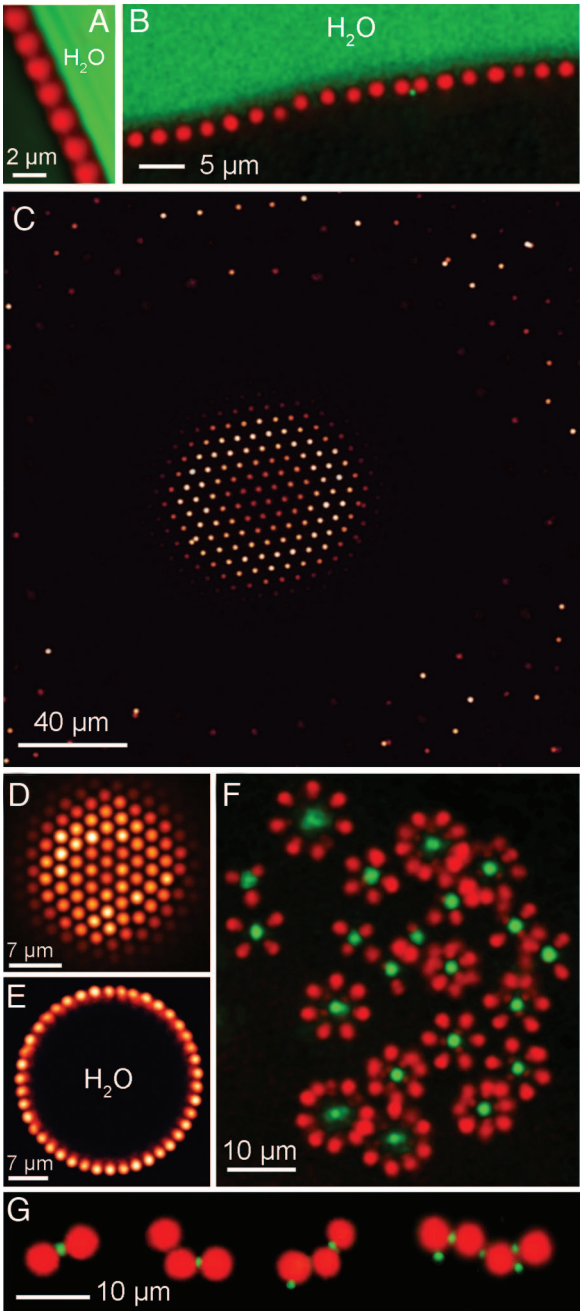

Fig. 2. PMMA particles (radius 1.08 μm) in CHB-decalin permanently bound at the oil-water interface in various configurations. (*A* and *B*) Close-up images perpendicular to the interface. The water phase was imaged in bright-field transmission mode (green color table) (*A*) or by dissolving fluorescent dye in it (*B*). (*C*) Top surface of a hemispherical water droplet on the sample cell wall (as seen from the oil phase). Note the depleted zone in the oil phase. (*D* and *E*) Free-floating spherical water droplet covered by a hexagonal lattice of particles. Shown is the surface (*D*) and is a slice through the center (*E*). (*F*) Small water droplets (green) covered with particles (this is a cut through their centers). (*G*) Very small, fluorescently labeled water droplets (green) linking together PMMA particles.

small, negatively charged clusters that bind to like-charged NaOH-containing water droplets (pH 9.5), although their macroscopic contact angle is 180° (Fig. 3*C*). In another system, consisting of octadecanol-coated silica particles (a_c = 215 nm) in CHB or chloroform, the particles also have a large contact angle and are positively charged. They bind both to like-charged water and glycerol droplets, forming a 2D hexagonal crystal with large lattice spacing, similar to those formed by PMMA particles as described below (however, upon prolonged exposure to water the silica particles reverse their charge and aggregate, likely because of hydrolysis of the octadecanol coating).

Recognition of this ability to bind nonwetting and like-charged particles to interfaces and the realization that image charge effects are also important for wetting particles (where it comes on top of a surface tension effect) are essential for a full understanding of particle-stabilized emulsions. More generally, these often-overlooked image charge interactions could play an important role in any system where charges reside near an interface between different dielectric constant media. For instance, it was recently shown that a halo of highly charged nanoparticles can stabilize much larger colloids (26–28). For the systems in ref. 26, the interaction between the nanoparticles and their image charge inside the colloids is repulsive and hence would not change the qualitative behavior (but it would quantitatively). However, for systems with inverted dielectric constant contrast of the colloids and the suspending medium, image charge attractions could make the nanoparticle halo "collapse" onto the colloids.

Exploiting the acquired insight in the electrostatic interactions between oil–water emulsions and colloids, we made a diversity of interesting structures, thus demonstrating the additional control they offer. Fig. 2*C* shows a hemispherical water droplet on the sample cell wall. The particles in the oil near the interface are attracted by their image charges and then trapped by image charge and wetting forces (if any). The electrostatic interparticle repulsion leads to a hexagonal "surface crystal" with large lattice spacing. As expected, there is a well defined depleted zone, separating the surface crystal from the 3D Wigner crystal of particles in the oil phase. This spatial separation allows us to precisely control the interfacial particle density by applying a dc electric field, which draws the charged colloids through the depleted zone [see supporting information (SI) Movie 1]. Fig. 2 *D* and *E* shows a similar, but denser, particle arrangement on the surface of a free-floating, spherical water droplet. As Fig. 2*F* demonstrates, even tiny droplets can carry many particles. However, when we make them smaller than the colloidal particles, the electrostatic interparticle repulsion becomes increasingly important, limiting the number of attracted particles to two. The result is chains of alternating particles and water droplets (Fig. 2*G*).

Our system easily forms the other, oil-in-water, Pickering emulsion as well, thereby forming one of the exceptions to Bancroft's rule (29), which implies that the liquid least wetting the particles tends to form the disperse phase. Fig. 4 and SI Movie 2 show a scan through such a colloidal particle-containing oil droplet in the bulk water phase. The particle monolayer on the inner surface, the small depleted zone, and the finite-size Wigner crystal in the center are clearly distinguishable. Particularly striking is that the encapsulated crystal undergoes free Brownian rotations relative to the surrounding shell. This rotational freedom suggests an interesting packing problem: the observed ordering for two, three, four, . . . particles is the optimum configuration for a finite Coulomb crystal in a spherical potential well. It also enables investigations of the one-component plasma limit in strongly confined geometry.

Obviously, if the ion drainage and self-charging through preferential partitioning are intrinsic properties of oil–water mixtures, then we should see these effects without colloidal particles, too. The case is clearly made in Fig. 5 *A* and *B*. Here, we added a small amount of water (5% by weight) to CHB and dispersed it by using a sonication bath for 2 min. We observed the rapid formation of a water-in-oil emulsion with droplet diameters of up to 3 μm. Although we did not add any emulsifiers, the droplets were stable for many months, as ob-

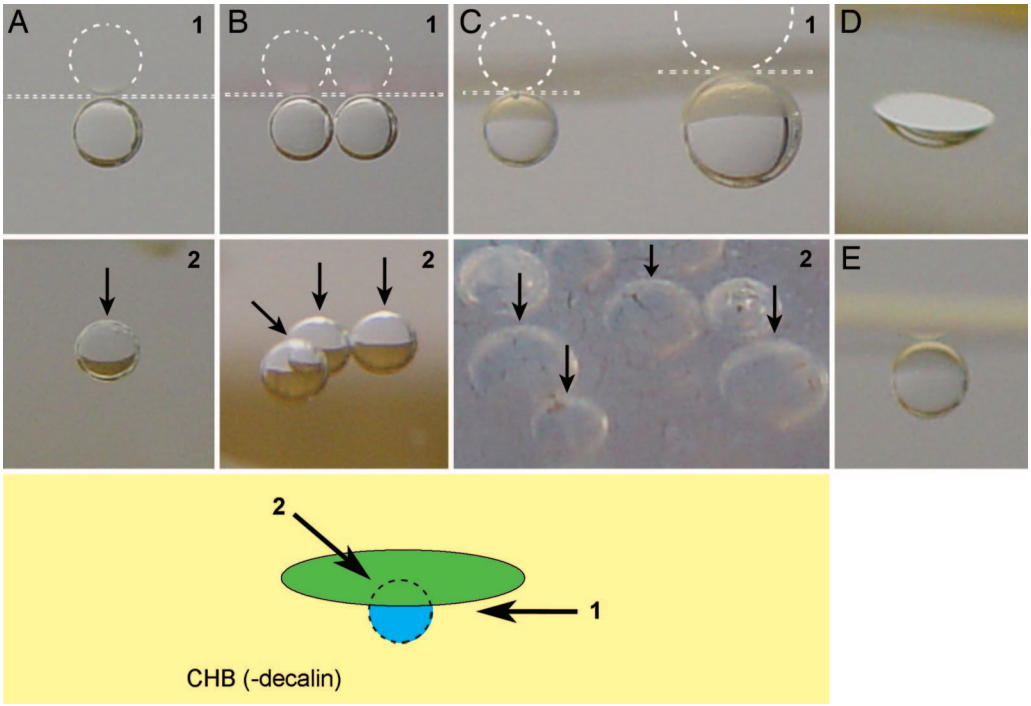

Fig. 3. Macroscopic contact angle measurements. (*A–C*) Digital photographs of 1- to 2-mm-sized water droplets buoyantly pressing against the bottom side of glass coverslips, coated with a homogeneous layer of poly(12-hydroxystearic acid)-PMMA (deposited from chloroform) and then submerged in CHB-decalin (*A*), coated with fluorescently labeled PMMA particles (radius 1.08 μm) melted together and then submerged in CHB-decalin (*B*), and coated with Hyflon Per-fluoro-alkoxy particles (radius ≈90 nm) and then submerged in pure CHB (*C*). The schematic drawing (*Bottom*) indicates the two different directions of viewing: perpendicularly from the side (image 1) or under a small angle from the top, through the transparent coverslip (image 2). In image 1, the exact position of the slide (indicated by a double dashed line) can be judged from the droplet's reflection (highlighted with a dashed line). In image 2, the arrows indicate the point of contact. All substrates are essentially nonwet. (*D* and *E*) For comparison we show a tilted top view of an uncoated glass coverslip (*D*), which is clearly wet, and a side view of a large solid Teflon sheet (*E*), which has a contact angle of 180°.

served by microscopy. The nature of their stabilization is evident from the micrographs: repulsive interactions prevent coalescence and are even sufficiently strong and long-range to cause crystallization (even despite the large polydispersity of the droplets). To the best of our knowledge this has not been reported before for additive-free systems. Judging by the nearly unaltered appearance even months after preparation the droplet charges are very stable.

In the same system we also find the other oil-in-water emulsion (Fig. 5*C*). Because water, with its shorter screening length, now forms the continuous phase, the droplets fail to crystallize and come much closer together. Nevertheless, the observed stability (weeks, months) is long in comparison to other additive-free oil-in-water emulsions (21, 30, 31).

The efficient stabilization solely by self-charging contradicts the common belief that stable emulsions require emulsifiers (1, 2) and is consistent with the pioneering investigations of Ellis (32). We successfully made charge-stabilized, crystal-forming water-in-oil emulsions with various solvents, but failed with some others (Table 1). Roughly, stable droplet arrays form if $4 < \varepsilon_{oil} < 10$. Likely because of a lack of spontaneous charge dissociation, droplets in less polar oils do not acquire enough charges, but one apparently can shift the lower limit down to $\varepsilon_{oil} \approx 1.5$ by adding charge-stabilizing surfactants (8). In recent years, this interesting "low-polar" regime, characterized by a powerful combination of spontaneous charge dissociation and long screening lengths, has been quickly uncovered for solid particle suspensions (4, 5, 9, 10), but it may well be as important to emulsions.

Finally, aside from the water droplet crystals with large lattice spacing, the CHB-based oil–water mixtures behave rather similar to our colloidal particle-containing emulsions in several other respects. For example, we observe depleted zones, where small droplets are repelled by a large water–oil interface, and small water droplets inside a bigger CHB bubble (residing in a water bulk) forming confined Wigner structures (Fig. 5*D*).

Conclusions

Our findings clearly demonstrate the important role that (preferential) ion partitioning and other electrostatic effects can play

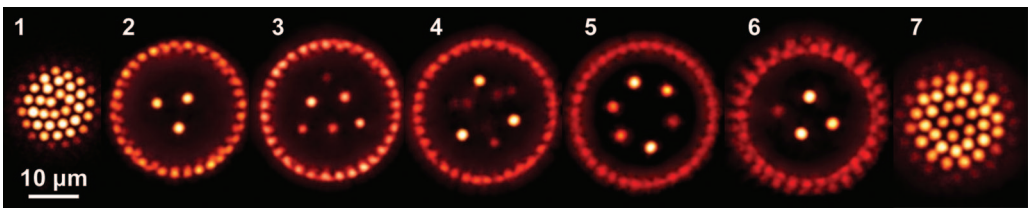

Fig. 4. Sequence of confocal slices through a colloidal particle-containing oil droplet (CHB-decalin) in water. There is a 2D crystal near the inner surface and a freely rotating, 3D Wigner crystal of 12 particles in the interior. Slices 3 and 5 lie halfway between successive particle planes.

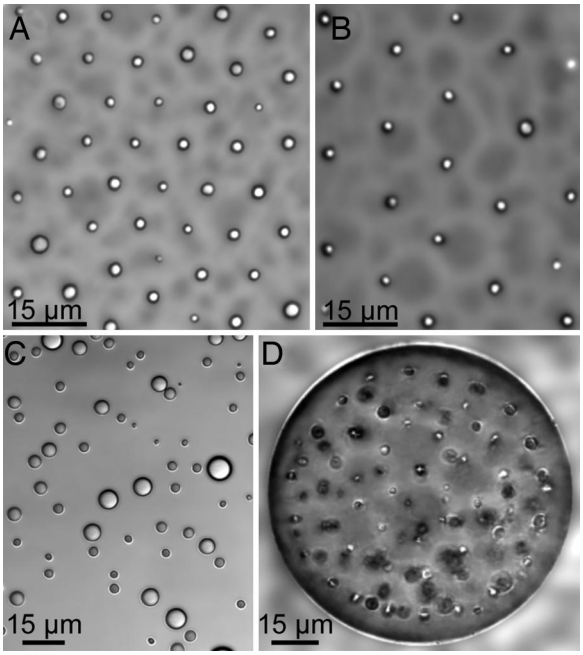

Fig. 5. Bright-field transmission images of charge-stabilized, additive-free emulsions. (*A* and *B*) Water droplets in CHB (*A*) and CHB-decalin (*B*) after 2 min of sonication, near the top wall of the sample cell (this is one layer of the 3D crystal). (*C*) CHB droplets in water, near the bottom of the sample cell. (*D*) Wigner crystal of small water droplets inside a bigger CHB droplet (in water). Note that curvature effects distort the image and that some droplets are not in focus.

in emulsions and colloids, especially those in which the continuous medium is a low polarity solvent. Despite their conceptual simplicity and utility these effects have received little attention before. Their practical power for manipulating certain systems is not only of interest for (self-) assembly (33, 34), but also for processes like emulsion production and encapsulation (33, 35). Moreover, the present results also provide us with a versatile model system in which we can easily control the number of colloidal particles residing at the oil–water interface, without the need for so-called "spreading agents." This finding could be useful in the ongoing investigations of the interactions between interfacial particles (25, 36) and their dynamics (37). From a more applied perspective it is interesting to note that the interfacial particles remain mobile. Thus a "line" of water could serve as a particle transport conduit (see SI Movie 3), which is useful for separations or separate particle and fluid control in microfluidics.

Table 1. Preparation of additive-free water-in-oil emulsions

Solvent	Dielectric constant, ε_{oil}*	Stable, crystal-forming droplets?
Dodecane	2.0	No
Cyclohexane	2.0	No
Bromoform	4.3	Yes
Chloroform	4.7	Yes
Dichloromethane	8.9	Yes
1-Butanol	17.3	No
cis-Decalin	2.2	No
Decalin-CHB 30% (by weight)	3.5	No
Decalin-CHB 50%	4.5	Repulsive droplets, but no crystal
Decalin-CHB 75%	6.0	Yes
CHB	7.9	Yes

*Exact value only known for the pure solvents. For the mixtures it was estimated based on the partial volumes of the components.

Materials and Methods

Particles. We used PMMA spheres, made by dispersion polymerization, sterically stabilized with covalently bound poly(12-hydroxystearic acid) and covalently labeled with the fluorophore rhodamine isothiocyanate (RITC). After the synthesis we washed the particles extensively with hexane and petroleum ether to remove any unreacted species. The particle radius was 1.08 μm with a polydispersity of 3%, as determined by static and dynamic light scattering (38). We also used the RITC-labeled octadecanol-coated silica particles of Verhaegh and van Blaaderen (39), which had a radius of 215 nm and 5.5% polydispersity (from light scattering and transmission electron microscopy), and Hyflon Per-fluoro-alkoxy polymer particles [kindly provided by S. Sacanna (Utrecht University), who obtained them as a donation from Ausimont Inc., Milan, Italy] with a (hydrodynamic) radius of ≈90 nm (40).

Suspensions. To avoid surface active contaminants we cleaned all glassware by sonicating it three times for 20 min with first chloroform, then absolute ethanol and finally deionized water, after which it was left to dry. The dry particles were dispersed in nearly density and index matched mixtures of CHB (Sigma–Aldrich, Zwyndrecht, The Netherlands) and 27.2 wt% cis-decalin (Sigma–Aldrich), avoiding sonication. Unless indicated otherwise, we used purified CHB for our experiments. The purification was done by washing with deionized water, followed by drying with $CaCl_2$ powder.

Confocal Microscopy. All samples were confined to glass capillaries with inner dimensions of 0.1 × 1 or 0.1 × 2 mm (VitroCom, Mountain Lakes, NJ) before studying them by confocal laser scanning microscopy. We used a NT and a SP2 setup (Leica, Ryswyk, The Netherlands) with N.A. 1.4 ×100, N.A. 1.3 ×63, and N.A. 1.25 ×40 oil immersion objectives (Leica). We used fluorescence mode, exciting the RITC-labeled particles with a 568-nm (NT) or 543-nm (SP2) laser line. The images were taken at low intensities (<100 μW) to prevent bleaching of the RITC dye and possible light-induced decomposition of the CHB solvent. We recorded *xy* images of 512 × 512 and 1,024 × 1,024 pixels, which took ≈1–2 s per frame. For 3D data we took stacks of *xy* slices spaced ≈400 nm apart (i.e., about five slices per particle diameter).

Electrical Conductivity Measurements. To estimate the ionic strength of the oily CHB phase we measured its conductivity with a model 627 instrument (Scientifica, East Sussex, UK). With the cup-type probe each measurement requires ≈4 ml of solvent. We then calculated the screening length by applying Walden's rule (5), using literature values for the ions' limiting equivalent conductances in water. The solvent mixture had a viscosity of 2.217 centipoise at 25°C (measured with a ViscoSystem; Schott, Mainz, Germany) and a dielectric constant of 5.59 (determined through correlation with the measured refractive indices of the mixture and the pure solvents).

Electrophoretic Mobility Measurements. The particle charge was quantified by means of electrophoresis (Delsa 440SX; Coulter, Mijdrecht, The Netherlands) on dilute suspensions (volume fraction 0.0015) in the CHB–decalin mixture, using the procedure developed by Kornbrekke *et al.* (41) and used by us before (5). Unfortunately, we did not have the proper experimental equipment to quantify the charge of the water and oil emulsion droplets, but we were able to determine the sign of their charge by applying an electric field, while looking at the direction of the droplet's electrophoretic motion with the microscope. In this

case the sample cell consisted of a 0.1 × 2-mm capillary with two 50-μm-diameter nickel alloy wires (Goodfellow, Huntingdon, U.K.), bent into a 90° angle, at the opposing ends.

Contact Angle Determination. To determine the extent of wetting of the PMMA particles at the oil–water interface we let the suspension and water form a vertical interface perpendicular to two horizontal cover slips spaced 10–20 μm apart. We then took images of this meniscus halfway between the two walls with both pure water and in the presence of a low concentration of FITC dye, using respectively transmission and fluorescence mode imaging (in both cases the RITC-labeled particles were imaged in fluorescence mode). The FITC dye did not have any noticeable effect on the behavior.

For a more precise measurement of the three-phase contact angle, we deposited subsequent layers of PMMA (from particles dissolved in chloroform) and poly(12-hydroxystearic acid) on a glass coverslip by spincoating. For comparison, we prepared another coverslip by depositing a monolayer of particles from CHB–decalin and then melting them together on a hot plate, so that the surface groups were the same as on the original colloidal particles. We submerged both slides in CHB–decalin and measured the contact angle in photographs of differently sized water droplets buoyantly pressing against these substrates. A similar determination was done for slides covered with Hyflon Perfluoro-alkoxy particles in pure CHB. The particle layer was deposited by drying from CHB and then rinsed three times with pure CHB to remove loose particles. The result was a slightly rough, but rather coherent, particle film.

We thank D. Derks for particle synthesis; the Physical and Colloid Chemistry Group at Utrecht University for access to its Delsa 440SX; and R. P. A. Dullens, B. P. Binks, and especially W. B. Russel for helpful discussions. This work was supported by the Stichting voor Fundamenteel Onderzoek der Materie, the Nederlandse Organisatie voor Wetenschappelijk Onderzoek, the National Aeronautics and Space Administration, and the National Science Foundation.

1. Becher P (1977) *Emulsions: Theory and Practice* (Krieger, New York).
2. Binks BP, ed (1998) *Modern Aspects of Emulsion Science* (R Soc Chem, Cambridge, UK).
3. Aveyard R, Binks BP, Clint JH (2003) *Adv Colloid Interf Sci* 100–102:503–546.
4. Yethiraj A, van Blaaderen A (2003) *Nature* 421:513–517.
5. Royall CP, Leunissen ME, van Blaaderen A (2003) *J Phys Condens Matter* 15:S3581–S3596.
6. Hsu MF, Dufresne ER, Weitz DA (2005) *Langmuir* 21:4881–4887.
7. van der Hoeven PC, Lyklema J (1992) *Adv Colloid Interf Sci* 42:205–277.
8. Ryoo W, Webber SE, Bonnecaze RT, Johnston KP (2006) *Langmuir* 22:1006–1015.
9. Leunissen ME, Christova CG, Hynninen A-P, Royall CP, Campbell AI, Imhof A, Dijkstra M, van Roij R, van Blaaderen A (2005) *Nature* 437:235–240.
10. Shevchenko EV, Talapin DV, Kotov NA, O'Brien S, Murray CB (2006) *Nature* 439:55–59.
11. Chu JH, Lin I (1994) *Phys Rev Lett* 72:4009–4012.
12. Verwey EJ, Overbeek JT (1948) *Theory of the Stability of Lyophobic Colloids* (Elsevier, New York).
13. Marcus Y (1985) *Ion Solvation* (Wiley, Chichester, UK).
14. Lyklema J (1995) *Fundamentals of Interface and Colloid Science* (Academic, London).
15. Volkov AG, Deamer DW, Tanelian DL, Markin VS (1998) *Liquid Interfaces in Chemistry and Biology* (Wiley, New York), pp 136–139; 192–217.
16. Starks CM, Liotta CL, Halpern M (1994) *Phase-Transfer Catalysis* (Chapman & Hall, New York).
17. Zhan C-G, Dixon DA (2002) *J Phys Chem A* 106:9737–9744.
18. Zhan C-G, Dixon DA (2001) *J Phys Chem A* 105:11534–11540.
19. Haughey D, Earnshaw JC (1996) *Colloids Surf A* 106:237–242.
20. Marinova KG, Alargova RG, Denkov ND, Velev OD, Petsev DN, Ivanov IB, Borwankar RP (1996) *Langmuir* 12:2045–2051.
21. Beattie JK, Djerdjev AM (2004) *Angew Chem Int Ed* 43:3568–3571.
22. Pickering SU (1907) *J Chem Soc* 91:2001–2021.
23. Jackson JD (1999) *Classical Electrodynamics* (Wiley, New York).
24. Danov KD, Kralchevsky PA, Ananthapadmanabhan KP, Lips A (2006) *Langmuir* 22:106–115.
25. Aveyard R, Binks BP, Clint JH, Fletcher PDJ, Morozov TS, Neumann B, Paunov VN, Annesley J, Botchway SW, Nees D, *et al.* (2002) *Phys Rev Lett* 88:246102-1.
26. Tohver V, Smay JE, Braem A, Braun PV, Lewis JA (2001) *Proc Natl Acad Sci USA* 98:8950–8954.
27. Karanikas S, Louis AA (2004) *Phys Rev Lett* 93:248303.
28. Liu J, Luijten E (2004) *Phys Rev Lett* 93:247802.
29. Bancroft WD (1913) *J Phys Chem* 17:501–519.
30. Pashley RM (2003) *J Phys Chem B* 107:1714–1720.
31. Sakai T, Kamogawa K, Harusawa F, Momozawa N, Sakai H, Abe M (2001) *Langmuir* 17:255–259.
32. Ellis R (1912) *Zeit Phys Chem* 80:597–616.
33. Hsu MF, Nikolaides MG, Dinsmore AD, Bausch AR, Gordon VD, Chen X, Hutchinson JW, Weitz DA, Marquez M (2005) *Langmuir* 21:2963–2970.
34. Velev OD, Furusawa K, Nagayama K (1996) *Langmuir* 12:2374–2384.
35. Gibbs BF, Kermasha S, Alli I, Mulligan CN (1999) *Int J Food Sci Nutr* 50:213–224.
36. Pieranski P (1980) *Phys Rev Lett* 45:569–572.
37. Lipowsky P, Bowick MJ, Meinke JH, Nelson DR, Bausch AR (2005) *Nat Mater* 4:407–411.
38. Bosma G, Pathmamanoharan C, de Hoog EHA, Kegel WK, van Blaaderen A, Lekkerkerker HNW (2002) *J Colloid Interf Sci* 245:292–300.
39. Verhaegh NAM, van Blaaderen A (1994) *Langmuir* 10:1427–1438.
40. Koenderink GH, Sacanna S, Pathmamanoharan C, Rasa M, Philipse AP (2001) *Langmuir* 17:6086–6093.
41. Kornbrekke RE, Morrison ID, Oja T (1992) *Langmuir* 8:1211–1217.